International Journal of Pharmaceutics 429 (2012) 138–147

Contents lists available at SciVerse ScienceDirect

International Journal of Pharmaceutics

journal homepage: www.elsevier.com/locate/ijpharm

Mesoporous silica nanoparticles for the improved anticancer efficacy of cis-platin

Chia-Hui Lin[a], Shih-Hsun Cheng[a], Wei-Neng Liao[a], Pei-Ru Wei[a], Ping-Jyun Sung[b], Ching-Feng Weng[a], Chia-Hung Lee[a,*]

[a] Department of Life Science and Institute of Biotechnology, National Dong Hwa University, Hualien 974, Taiwan
[b] Graduate Institute of Marine Biotechnology, National Dong Hwa University, Pingtung 944, Taiwan

ARTICLE INFO

Article history:
Received 23 December 2011
Received in revised form 13 February 2012
Accepted 15 March 2012
Available online 23 March 2012

Keywords:
Drug delivery
Anticancer
Cis-platin
Controllable release

ABSTRACT

We designed a novel cis-platin (CP) delivery system by modification of mesoporous silica nanoparticle (MSN) surfaces with a carboxylate group through a hydrazone bond. The further immobilization of CP can be achieved through the coordination of the carboxylate-modified MSN surfaces with the hydroxo-substituted CP. This new formulation can efficiently increase efficiency of both the cellular uptake and the drug release under endosomal or lysosomal pHs; therefore, the anti-proliferative effect of this new formulation on the colon cancer cell line (HT-29) was twenty times more than the free CP molecules. In addition, the encapsulation of CP complexes in the confined spaces of MSNs can decrease non-specific release from enzymatic hydrolysis because most hydrolytic enzymes have diameters considerably greater than the pore size of MSNs. The DNA fragmentation and caspase-3 activity assay showed that the apoptosis was induced by DNA damages and then an increase in caspase-3 activity. Thus, the TA-MSN-carboxylate-CP samples were induced cell apoptosis through the caspase-3 dependent pathway. Moreover, the hemolysis assay also indicated that the exposure of the carboxylate-modified MSNs in red blood cells (RBCs) did not observe the release of red hemoglobin from the cell lysis, and the further exposure of the TA-MSN-carboxylate-CP complexes to RBCs also did not observe notably the lysis of RBCs under the effectively therapeutic dosage. Therefore, our design of MSN with controllable release of CP has highly therapeutic effects and is highly biocompatible; however, a low cytotoxicity and site effect were observed.

1. Introduction

In recent years, there has been a growing trend of people suffering from malignant cancer and this disease has become one of the major causes for death worldwide. Many researches have attempted to develop an efficient approach to cure and prevent cancer. For a novel therapeutic strategy, the use of nanoparticles as a drug delivery system can provide a possible opportunity, which can deliver drug molecules to the targeting site through the nanoparticle formulation (Ferrari, 2005); therefore, an enhancement of therapeutic efficiency by selectively increased local drug concentration in the tumor tissues can be easily achieved. The nanoparticle drug delivery system has the advantages of accumulating large amounts of therapeutic drugs in the tumor tissues through the passive and active targeting approach (Wu et al., 2011). For passive tumor targets, nanoparticles can increase selectivity and the local concentration in the tumor by the enhanced permeability and retention effect (EPR effect), which can target the high permeability of leaky microvessels from the tumor angiogenesis (Brigger et al., 2002). Regarding the active target, the nanoparticle surfaces are functionalized with targeting molecules; therefore, the nanoparticles can interact with the over-expression of specific receptors in the cancer cell surfaces (Ferris et al., 2011).

In recent years, interest in inorganic materials has arisen in the fields of chemical, biological, and drug delivery applications. Particularly, the Mesoporous silica nanoparticles (MSNs) have recently generated vast amounts of studies for use as a novel delivery vehicle (Mamaeva et al., 2011) and an in vivo contrast agent (Hsiao et al., 2008; Kim et al., 2008; Lebret et al., 2010; Lee et al., 2010) to accurately control the release of therapeutic drugs (Rosenholm et al., 2010) and genes (Suwalski et al., 2010; Torney et al., 2007). Because of the large surface areas, large pore volumes, highly ordered pore structures, and adjustable pore sizes, mesoporous silica has wide and interesting applications as a support for chemical and biological catalysts. For drug delivery applications, the abundant silanol groups (Si—OH) that tile their pore surfaces facilitate mesoporous silica post-synthesis modification with various organic linkers, thereby simplifying the design of controlled-release mechanisms and targeting approaches for the decrease of systemic toxicity and side effects. Several research groups have also studied the sustained-release properties of drugs loaded in various mesoporous based materials such as MCM41S (Sun et al., 2009), SBA

* Corresponding author. Tel.: +886 3 863 3682; fax: +886 3 863 3630.
E-mail address: chlee016@mail.ndhu.edu.tw (C.-H. Lee).

0378-5173/$ – see front matter © 2012 Elsevier B.V. All rights reserved.
doi:10.1016/j.ijpharm.2012.03.026

(Chen et al., 2011b), HMS (Wang, 2009), TUD (Heikkila et al., 2007), FDU (Hartono et al., 2009), and MSU families (Tourne-Peteilh et al., 2003). Different types of mesoporous materials with various pore structures, pore sizes and surface functionality were designed for the drug formulations which can enhance absorption of the poorly soluble drug (Zhang et al., 2011) and provide sustained drug release (Van Speybroeck et al., 2010). Vallet-Regi et al. have reported that these versatile hosts can be applied to implantable, oral, transdermal, injectable drug reservoirs (Vallet-Regi et al., 2007), and for bone tissue regeneration (Vallet-Regi et al., 2008). Simply for drug loading, the drug molecules can be adsorbed inside the non-functionalized silica matrix through hydrogen bonding attractions; however, the low affinity usually caused low loading amounts and the burst release of the pre-loaded drug molecules. To increase the drug loading amounts and regulate the releasing profile, the silica surfaces can be further modified with ionic charges which can increase the electrostatic attractions between the carrier surfaces and the opposite charges of the drug molecules (Chang et al., 2010). Another approach to stabilize the immobilized drug molecules in the mesoporous silica surfaces can employ the surface modification of an organic linker, which can tether the drug molecule through a covalent conjugation. The conjugated groups between the organic linker and the drug molecule can be designed for different release mechanisms such as pH variation (Knezevic et al., 2011), temperature regulation (Liu et al., 2009), light irradiation (Aznar et al., 2009), electrostatic repulsion (Lee et al., 2008), magnetic field perturbation (Hu et al., 2008) or enzymatic cleavaged release (Coll et al., 2011; Sauer et al., 2010). In addition to the sustained and spontaneous release systems, the stimuli-responsive release systems have been widely studied recently (Gao et al., 2009); for example, a cap formed (Wang et al., 2010; Zhao et al., 2010) by a cleavage bond (Chen et al., 2011a; Giri et al., 2005) or a dissoluble substance (Muharnmad et al., 2011; Yuan et al., 2011) can be opened by the biological environments to trigger the release of the entrapped molecules (Bernardos et al., 2010; Gan et al., 2011). The pH stimuli-responsive controlled release systems (Gao et al., 2010b; Sun et al., 2010) composed of oppositely charged ionic interactions between the modified mesoporous silica surfaces and the organic molecules have also been studied (Cauda et al., 2010; Yang et al., 2005). A novel pH responsive controlled release system based on the coordination bonding of metal ions and functional groups in mesoporous silica has also reported recently (Gao et al., 2010a; Zheng et al., 2011). In addition to the solid mesoporous silica, a hollow mesoporous silica nanosphere with pore channels penetrating from the outside to the inner hollow core can store significantly more drug molecules than conventional mesoporous silica (Wang et al., 2011). For the design of various releasing mechanisms, the use of pH dependent release has great potential in cancer therapy because the tumor tissues and the endosomal (or lysosomal) environments have more acidic pH values (Gao et al., 2010b). From this advantage, many studies have reported the combination of pH-sensitive and pro-drug strategies through the conjugation of cytotoxic drug in a carrier surface which can increase tumor targeting, decrease side effects and the systemic toxicity of traditional chemotherapy (Song et al., 2007). The conjugation of anticancer drugs to a polymer backbone or nanoparticle surfaces by active bonds, such as acetal (Schlossbauer et al., 2011), hydrazone (Etrych et al., 2002), or ester bonds has been reported (Xue and Shi, 2004). Although a number of studies have confirmed endosomal release of the pH-sensitive formulation (Prabaharan et al., 2009), considerable extracellular pre-release of the drug from the hydrolysis of the drug-conjugating linker by enzymatic catalysis remains a problem. For this reason, we grafted the drug molecules in the nanochannels of MSN through a pH-sensitive bond which is inherently immune to enzymatic degradation and hydrolysis while enabling extraordinarily large loadings of drugs. The confined spaces of the nanochannels can provide steric barriers to enzyme entry and reaction, as most hydrolytic enzymes have diameters considerably greater than those of the traditional functionalized-MSN pores (2–3 nm). Therefore, drugs conjugated to the inner walls of the MSN nanochannels through a pH-sensitive bond are largely protected from extracellular hydrolysis and premature release. Furthermore, the acidic environments of endosomal or lysosomal pHs can diffuse protons into the nanochannels of MSNs and cleave the labile linker tethered in the internal walls of the nanochannels. Thus, the conjugation of drug molecules to MSN surfaces through a pH-sensitive linker can provide a sustained released property which can further decrease systemic toxicity by increasing tumor targeting while the reducing fluctuations of peaks of the unutilized drug in the extracellular plasma. In addition, the cellular uptake of MSNs can be well controlled through the regulation of the particle size and surface charges (Vallhov et al., 2007). When MSNs have diameters of between 50 nm and 100 nm and positively charged surfaces, they can readily undergo endocytosis in cancer cells with much higher cellular uptake efficiency than the passive transfer of free drug molecules by the simple diffusion across the cell membranes (Lu et al., 2009).

In this work, we reported a novel pH-sensitive release of cisplatin, a clinically used anticancer drug for widely treating various types of cancers, by the combination of a carboxylate group with a pH-sensitive hydrazone bond in the MSN surfaces. For traditional cancer therapy, CP has shown the severe drawbacks of low solubility, a lack of vivo circulation, organic toxicity and nerve damage. To overcome the drawbacks of CP, many researches have reported the incorporation of CP in organic and inorganic materials (biopolymers, dendrimer, carbon nanotube, and gold nanoparticles) through the physical adsorption (Tao et al., 2010) or coordination from the carboxylate group which can solve some of the disadvantages of systemic toxicity (Bhirde et al., 2009; Gu et al., 2010; Malik et al., 1999; Rieter et al., 2008; Uchino et al., 2005). Due to the good leaving group of carboxylate, the coordinated CP can be efficiently released through NAD(P)H-reductase, the high Cl^- concentration or H_2O in the cytosol (Taylor et al., 2010; Xie et al., 2010). For our approach, CP molecules can be stabilized by being tethered to MSN surfaces through the production of CP-carboxylate complexes inside the nanochannels. We further incorporated CP-carboxylate complexes with a pH-sensitive hydrazone bond to tether CP complexes to the internal surfaces of MSNs; therefore, the release of CP-carboxylate complexes from the endosomal (or lysosomal) environments of the tumor tissues was further enhanced in the pH range of 5.0. The combination of MSNs with a pH-sensitive release to deliver CP has the advantages of preventing extracellular pre-release of the CP from the enzymatic degradation and hydrolysis. Furthermore, an enhancement of CP release in the cancer cells can be achieved through (1) the pre-hydrolysis of hydrazone bond in endosomal (or lysosomal) environments, (2) the further reduction and release of CP molecules from the NAD(P)H-reductase and/or glutathione in the cytosol, and (3) the sustained release of CP molecules by the replacement of high Cl^- concentrations.

2. Materials and methods

2.1. Materials

Cetyltrimethylammonium bromide (CTAB), tetraethoxysilane (TEOS), ethanol, acetone, ammonium hydroxide (30%), and HCl (37%) were purchased from Acros. The n-octane was purchased from Alfa Aesar. Potassium hydrazinocarbonyl-acetate, cis-platin, $AgNO_3$, acetic acid, trichloroacetic acid, sulforhodamine B, and

trizma base were purchased from Sigma. Triethoxysilylbutyraldehyde, N-trimethoxysilylpropyl-N,N,N-trimethyl-ammonium chloride (50% in methanol) was obtained from Gelest. A RPMI-1640 medium, fetal bovine serum, penicillin, and streptomycin were obtained from GIBCO/BRL Life Technologies (Grand Island, NY, USA). A Genomic DNA purification kit was obtained from Promega (Madison, WI). A caspase-3 colorimetric assay kit was obtained from R&D Systems Inc. RBCs (goats) were a gift from the Hualien District Agricultural Research and Extension Station, Taiwan.

2.2. Incorporation of trimethylammonium (TA) groups in the frameworks of MSN (TA-MSN)

Large pore diameters of MSN samples with hexagonal well ordered pore structures and TA-modified frameworks were synthesized in a low concentration TEOS, surfactant (CTAB), trimethylammonium silane and base catalyst (NH_4OH) under a two-step preparation (Lin et al., 2005). The sol–gel process, for the co-condensation of TEOS to synthesize TA-MSN, was as follows. First, CTAB (0.58 g) was dissolved in NH_4OH (0.51 M, 300 mL) at 40 °C and 5.0 g of the structural swelling agent (n-octane) was then added. After stirring for 1 h, 5 mL of 0.2 M TEOS (in ethanol) was added with vigorous stirring. After the solution was further stirred for 5 h, 5 mL of 0.2 M trimethylammonium silane (in ethanol) was added and stirred for 5 min; and further, 5 mL of 1.0 M TEOS (in ethanol) was added with vigorous stirring for another 2 h. The solution was aged at 40 °C for 20 h. Samples were collected by centrifuging at 12 000 rpm for 20 min, washed, and redispersed in deionized water and ethanol three times. The solid products were obtained by centrifugation and the surfactant templates were removed by extraction in acidic ethanol (one batch of as-synthesized MSN in 1.0 g of 37% HCl and 50 mL of ethanol (99.5%) at 65 °C for 24 h). Further, nanoparticles were collected and washed with 20 mL ethanol three times.

2.3. Synthesis of aldehyde-modified TA-MSN

The anchoring of aldehyde groups onto the surfaces of TA-MSN was accomplished as follows. First, 200 mg of the extracted TA-MSN was placed in 50 mL of toluene and stirred for 30 min. Then, 1.0 mL of triethoxysilylbutyraldehyde was then added to the resulting suspension and allowed to react for 20 h at 80 °C. Samples were collected by centrifuging at 12 000 rpm for 20 min, washed, and redispersed in acetone several times.

2.4. Conjugation of hydrazinocarbonyl acetate in aldehyde modified TA-MSN

Conjugation of pH-sensitive carboxylate groups on aldehyde-modified TA-MSN surfaces was achieved through the nucleophilic addition of the aldehyde and hydrazinocarbonyl acetate groups to produce a hydrazone bond. The reaction conditions were as follows. First, 10 mg of aldehyde-modified TA-MSN was suspended in 1.0 mL of anhydrous methanol. Next, 5.0 mg of potassium hydrazinocarbonyl-acetate was added to the above solution, followed by one drop of acetic acid. The solution was then shaken at room temperature for 24 h. The solids of pH-sensitive carboxylate-modified TA-MSN samples were isolated by centrifuging at 12 000 rpm for 20 min, washed, and redispersed in methanol several times.

2.5. Coordination of CP onto the pH-sensitive TA-MSN-carboxylate samples

To increase the reactive concentration of CP in aqueous solution, the chloro ligand of the CP molecules was replaced by the hydroxo ligand through the reaction of CP (20 mg) in $AgNO_3$ solution (23 mg in 1.5 mL dd-H_2O) under 37 °C and kept dark for 12 h. After the reaction, an AgCl precipitation was produced and the solution was then centrifuged for 20 min at 12 000 g to remove the precipitate. The supernatant containing highly water soluble CP adjusted its pH value to 7.2 and was then diluted to 4 mL by the addition of dd-H_2O. The TA-MSN-carboxylate CP complexes were synthesized by the addition of pH sensitive TA-MSN-carboxylate samples (8 mg) in 2 mL of CP solution, the mixtures were shaken under 37 °C and kept dark for 12 h and the TA-MSN-carboxylate-CP solids and the un-coordination of free hydroxo-CP solution were separated by centrifuging at 12 000 rpm for 20 min and further washed, and redispersed in dd-H_2O several times. The conjugated amounts of cis-platin in the nanoparticles were determined by measuring the decrease of absorption at 276 nm. Calibration experiments were done separately before each set of measurements with cis-platin of different concentrations. The loading percentage of cis-platin in pH-sensitive TA-MSN-carboxylate samples was near 10.25% (w/w).

2.6. Cell culture

HT-29 (human colon cancer cell line) was cultured in an RPMI-1640 medium supplemented with 10% (v/v) fetal bovine serum and penicillin (100 units mL^{-1})/streptomycin (100 mg mL^{-1}). Cultures were maintained in a humidified incubator at 37 °C in 5% CO_2. Morphology of control cells and samples-treated cells were observed by optical microscope (Olympus).

2.7. Sulforhodamine B assay

1×10^4 HT-29 cancer cells were seeded onto 96-well plates containing RPMI-1640 medium with 10% fetal bovine serum and then further incubated in 5% CO_2 at 37 °C overnight. After cell attachment, one group of cell line was fixed in situ with 25 μL of 50% (w/v) trichloroacetic acid (TCA) to determine the cell number at the time the cells received the tested drug (T_0). For the other groups, various drug concentrations in serum free medium were added and incubated for 4 h and then the same volume of 20% FBS medium was added to treatment for 20 h (T_x groups). After 24 h of drug treatment, the T_x groups and the control group (Ctl: no drug treated wells) were added into cold TCA (50 μL) and incubated at 4 °C for 1 h. Further, the medium was removed by suction, and washed three times with dd-H_2O (200 μL each time), and then dried under air for 12 h. Then, 100 μL of 0.4% (w/v) sulforhodamine B solution prepared in 1% acetic acid was added to each well, and the plates were incubated for 20 min at room temperature. The unbound sulforhodamine B was removed and washed three times with 1% (v/v) acetic acid. The bound sulforhodamine B was subsequently soluble by addition of 10 mM of trizma base (pH 10.5), and the absorbance was measured at 515 nm. The percentage of growth inhibition was defined as $100 - [(T_x - T_0)/(\mathrm{Ctl} - T_0)] \times 100$ (when $T_x \geq T_0$). GI_{50} (concentration of 50% cell growth inhibition) was defined as $\{100 - [(T_x - T_0)/(\mathrm{Ctl} - T_0)] \times 100\} = 50$ and calculated by the SigmaPlot software.

2.8. DNA fragmentation assay

HT-29 cells (1×10^6/mL) were treated with or without drug for 24 h, washed with PBS twice, lysed in cell lysis solution, and then pipetted until no visible cell clumps remained. Genomic DNA was purified by the Wizard Genomic DNA purification kit. After isopropanol precipitation, samples of 10 μg in each lane were loaded. The pattern of DNA cleavage was analyzed by 2.0% agarose gel electrophoresis at 100 V for 1.5 h in Tris-borate/EDTA electrophoresis buffer.

2.9. Measurement of caspase-3 activity

To determine the caspase-3 activity, we used a commercial assay kit (caspase-3 colorimetric assay) from R&D Systems Inc. To analyze the increased enzymatic activity of the caspase-3 class of proteases in apoptotic cells by colorimetric reaction, we treated various concentration (10, 20, 50, 100, 200 μg/mL) of TA-MSN-carboxylate-CP for 24 h and then washed twice with PBS. Further, the cells were collected and centrifuged (250 g for 10 min) in a conical tube. The cell pellet was resuspended in cold lysis buffer (about 25 μL of lysis buffer per 1×10^6 cells). After incubated on ice for 10 min, cell homogenates were centrifuged at $10\,000 \times g$ for 1 min and transferred the supernate to a new tube and kept on ice. The protein content of the cell lysate was estimated using BCA Protein Assay. The enzymatic reaction for caspase activity was performed by reaction of cell lysate (50 μL with 200 μg of total protein) with 50 μL of reaction buffer containing 1% (v/v) of DTT stock and then 5 μL of Caspase-3 colorimetric substrate (DEVD-pNA) was added. The reaction mixture was incubated at 37 °C for 1 h, and then read the plate on a microplate reader using a wavelength of 405 nm.

2.10. Hemolysis assay

The method for hemolysis assay has been reported previously (Lin and Haynes, 2010). Heparin-stabilized goat blood samples were freshly obtained from the Hualien District Agricultural Research and Extension Station, Taiwan. A mixed sample of 5 mL blood and 10 mL PBS was centrifuged at $10\,000 \times g$ for 10 min, the pellet of RBCs was washed with PBS (10 mL) five times, and then 50 mL of PBS was added for further dilution. To evaluate the hemolysis of the various concentrations of nanoparticle exposure, the leach of red hemoglobin in the supernatant was determined by measurement of the absorption from the positive and negative control experiments by incubation of RBCs with dd-H_2O and PBS, respectively. The treated condition was as the following. A 200 μL of diluted RBC suspension was added into 800 μL of different concentrations of MSN in PBS solution by vortex and then the mixture samples were kept at room temperature for 3 h. After the nanoparticle treatment, the mixtures were centrifuged at $10\,000 \times g$ for 3 min, and a 100 μL of supernatant from each treatment was transferred to a 96-well plate. Absorbance was measured using a micro plate reader set at 570 nm. Background correction was performed at 655 nm. The hemolysis percentages of RBCs were defined as:

$$\text{Hemolysis}\ (\%) = \frac{\text{sample absorption} - \text{negative control absorption}}{\text{positive control absorption} - \text{negative control absorption}} \times 100$$

2.11. Characterization

FT-IR spectra were recorded on a Nicolet 550 spectrometer with a KBr pellet. Approximately 1 mg of a sample was mixed with 300 mg of dried KBr and then pressed. The zeta potentials of various MSN samples were measured in a Malvern Nano-HT Zetasizer. The ζ-potential distribution was obtained by an average of ten measurements. The samples were prepared at a concentration of 2 mg in 1 mL of dd-H_2O. The ζ-potential from different pH values (2–9) was measured by an auto-titration system.

3. Results and discussion

3.1. Preparation of TA-MSNs-hydrazone-carboxylate-CP complexes

As shown in Scheme 1, the synthesis of a pH-sensitive hydrazone bond of the carboxylate-modified TA-MSNs was achieved through the reaction of hydrazinocarbonyl acetate groups with the aldehyde-modified TA-MSN surfaces (Scheme 1a). The incorporation of TA groups in the frameworks of MSNs can increase the cellular uptake through endocytosis because the positive charges of TA groups have high affinity to the negative charged surfaces of cell membranes. When the TA-MSNs-hydrazone-carboxylate-CP complexes (Scheme 1b) inherently accumulate in the solid tumors through the EPR effect, CP-loaded TA-MSN complexes have been highly uptaken by the cancer cells and then a pH-sensitive linker of the hydrazone bond was cleaved at the endosomal or lysosomal pHs (Scheme 1c) to release the CP-carboxylate complexes from the nanochannels of TA-MSNs. Furthermore, the activation of the carboxylate CP complexes and the release of free CP molecules were achieved by the NAD(P)H-reductase or glutathione reduction. Other mechanisms to release active CP may come from the replacement of carboxylate coordination (a good leaving group) of CP complexes from a strong nucleophile such as the cytosol Cl^- ions (Scheme 1d) (Gu et al., 2010). The activation of CP molecules can further diffuse into the nucleus and covalently bind with the DNA bases. Afterward, the cross-linked DNA transforms the DNA conformation and influences the transcription and translation of the cancer cells leading to irreparable DNA damage and tending to apoptosis pathway.

3.2. Characterization of the functionalized MSN samples

To conjugate the carboxylate group through a pH-sensitive hydrazone bond and the further coordination with CP-complexes onto the nanochannels of MSN surfaces, we synthesized large pore TA-MSN samples (1200 $m^2\ g^{-1}$ and 5.2 nm) by addition of a swelling agent (n-octane). TEM images of TA-MSN-hydrazone-CP complexes (Fig. 1) show that the sample generally has a round shape and a uniform size, with average particle diameters of approximately 60 nm. By using n-octane as a swelling agent to expand the inner micelle space, the as-synthesized MSN possesses both large pore diameters and well ordered pore structures. The conjugation of the hydrazinocarbonyl-acetate linkers and the further immobilization of CP complexes onto the TA-MSN surfaces did not affect the morphology and structure of TA-MSNs. To confirm that the chemical bonds and the organic groups of our modifications existed in the MSN surfaces, we employed FT-IR spectroscopy. The FT-IR spectra of surfactant-extracted TA-MSNs (Fig. 2a) showed a broad band (2700–3800 cm^{-1}) from the O—H stretch of the absorbed H_2O. The bands at 1077 cm^{-1} (with a shoulder at 1200 cm^{-1}) and 796 cm^{-1} are assigned to Si—O—Si vibration. The band at 1637 cm^{-1} is presumably caused by H_2O deformation. The presence of ν(C—H) mode at 1485 and 2980 cm^{-1} after HCl–EtOH extraction indicated that the TA groups were indeed modified in the framework of MSNs by covalent bonding in the one step sol–gel process. The aldehyde-silane modified TA-MSN sample (Fig. 2b) displays C=O stretch modes at near 1720 cm^{-1}. Conjugation of potassium hydrazinocarbonyl-acetate groups in TA-MSN-aldehyde surfaces (Fig. 2c) through the formation of hydrazone bonds showed an overlapping vibration absorption of carboxylate (C=O) and imine (C=N) near 1662 cm^{-1}. Other vibrations of N—H (bend), C—N (stretch), C—H (bend) absorption were displayed at 1546 cm^{-1}, 1409 cm^{-1}, and 1386 cm^{-1}, respectively. Especially, the hydrazinocarbonyl acetate-modified TA-MSN surfaces showed strong N—H (stretch) at 2888 cm^{-1} and C—H (stretch) at 2937, and 2975 cm^{-1}, which indicated that the hydrazinocarbonyl acetate groups exhibited highly modified amounts in the TA-MSN surfaces. Furthermore, the coordination of CP molecules in carboxylate-modified TA-MSNs (Fig. 2d) caused a decrease of the π electron cloud from carboxylate (C=O) groups; thus, the decrease of bond order caused a low frequency shift from 1662 of no CP-coordinated (C=O) to 1597 cm^{-1} of CP-coordinated (C=O) and the peak was overlapping with the N-H (bend) at

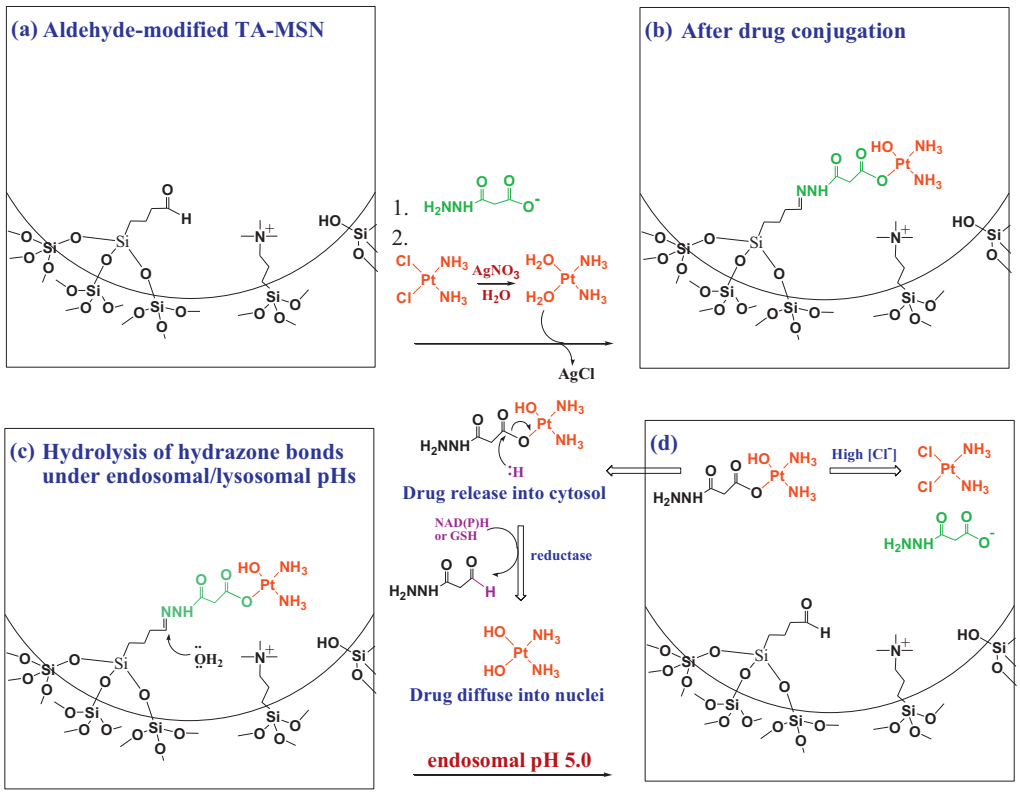

Scheme 1. The representation of the pH dependent release system of cis-platin immobilized on TA-MSN surfaces through a pH sensitive hydrazone bond: (a) aldehyde-modified TA-MSN surfaces, (b) the synthesis of a pH-sensitive carboxylate on TA-MSN surfaces through a hydrazone bond and the further immobilization of CP by chelation, (c) hydrolysis of a pH-sensitive hydrazone bond in the endosomal (or lysosomal) pHs, and (d) release of CP into cytosol by the helps of NAD(P)H-reductase, glutathione, or the high Cl^- concentration.

1546 cm^{-1}. After the hydrolysis of TA-MSNs-carboxylate-CP complexes at pH 5.0 for 12 h (Fig. 2e), the vibration absorptions of carboxylate (C=O) at 1597 cm^{-1} almost disappeared while the intensity of aldehyde groups (C=O) at 1720 cm^{-1} was increased. This phenomenon indicated that the pH-sensitive hydrazone bond in the carboxylate-modified TA-MSNs can be efficiently hydrolyzed under the treatment at the endosomal pH (5.0) for 12 h. To determine the loading percentages, we also measured the weight loss of the TA-MSNs complexes by thermogravimetric analyses (TGA) and the profiles were summarized in Fig. S1. The decomposition of TA-MSN complexes by the heating process mainly comes from the loss of adsorbed H_2O in the MSN surfaces and further weight loss may come from the combustion of organic ligands and the complexes of CP molecules. The TGA profiles of TA-MSNs only, aldehyde-modified TA-MSN samples, the conjugation of the hydrazinocarbonyl acetate ligands, and the further coordination of CP molecules showed a gradual increase of weight loss from 6% (Fig. S1a), 17% (Fig. S1b), 19% (Fig. S1c) to 26% (Fig. S1d), respectively. From the TGA results, we may confirm that the synthesis of organic ligands through the multi-step modification of TA-MSN samples was in actual existence in the MSN surfaces. To further confirm the hydrolysis of pH-sensitive hydrazone bonds of the

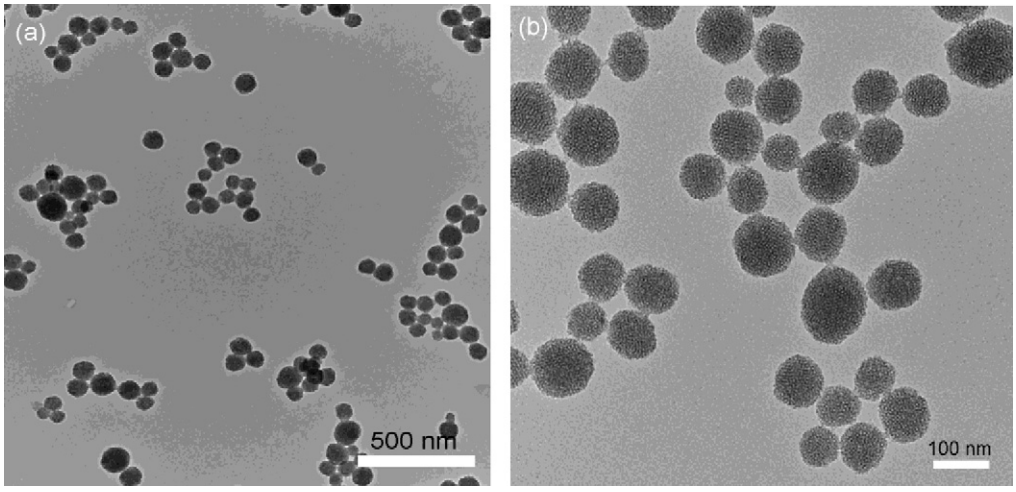

Fig. 1. TEM images of the characteristic round shape and the uniform size of TA-MSN-carboxylate-CP complexes. Scale bars: (a) 500 nm and (b) 100 nm.

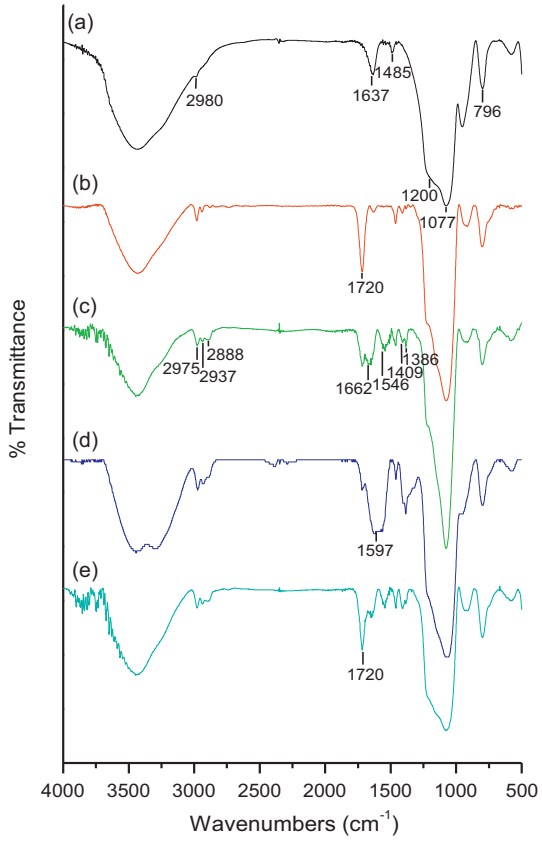

Fig. 2. FT-IR spectra of (a) TA-MSN, (b) TA-MSN-aldehyde, (c) TA-MSN-carboxylate, (d) TA-MSN-carboxylate-CP complexes, and (e) after hydrolysis of TA-MSN-carboxylate-CP complexes at pH 5.0 for 12 h.

TA-MSN-carboxylate-CP complexes under the endosomal pH (5.0), we measured the ζ-potential of TA-MSN-carboxylate-CP complexes before (Fig. 3a) and after hydrolysis (Fig. 3b) at pH 5.0 for 12 h. For ζ-potential measurements, the samples in dd-H_2O were titrated with the pH ranging from 2 to 9 automatically. The un-hydrolyzed TA-MSN-carboxylate-CP samples have a PZC (point zero charge) value at pH 5.1. After the hydrolysis of TA-MSN-carboxylate-CP samples at pH 5.0 for 12 h, we can observe

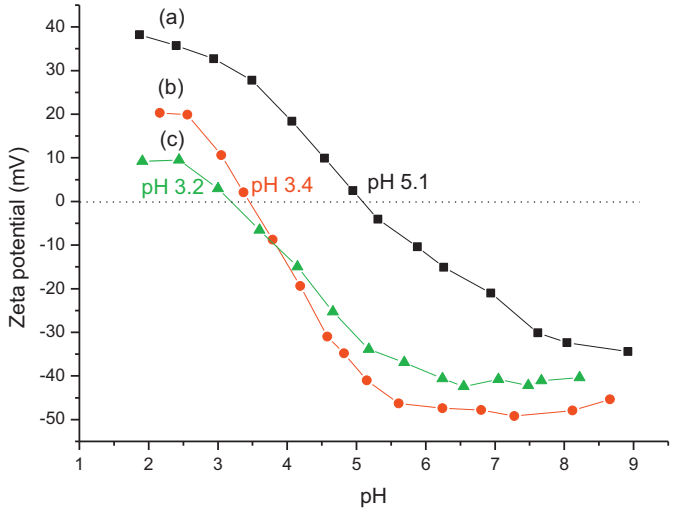

Fig. 3. Zeta potential of (a) TA-MSN-carboxylate-CP complexes, (b) after hydrolysis of TA-MSN-carboxylate-CP complexes under pH 5.0 for 12 h, and (c) aldehyde-modified TA-MSN.

that the PZC value of the hydrolyzed TA-MSN-carboxylate-CP samples (Fig. 3b) was shifted to 3.4, which nearly matched with the PZC value (pH 3.2) of the aldehyde-modified MSN sample (Fig. 3c). From the above results of ζ-potentials, we can infer that most carboxylate-CP complexes in the TA-MSN surfaces were fully hydrolyzed under endosomal pH for 12 h. Through the hydrolysis of hydrazone bond and the elimination of hydrazine-carboxylate-CP complexes, the TA-MSN-carboxylate-CP samples were restored to the initial surfaces of the aldehyde-modified TA-MSNs; therefore, the hydrolyzed products have approximate PZC values.

3.3. Anticancer activity studies

Fig. 4 shows the cell morphology before (Fig. 4a) and after the treatment of TA-MSN-carboxylate-CP complexes to HT-29 cancer cells for 24 h (Fig. 4b) at a concentration of 50 μg mL^{-1} (with 5.13 μg mL^{-1} free CP). Compared with the morphology of the cells without the drug treatment, we can observe that the TA-MSN-carboxylate-CP complexes treated cells had become round and had shrunk which is a typical phenomenon of cell apoptosis. In the treatment of the free CP molecules, the cell morphology was rarely round and shrunken even though a very high concentration (20 μg mL^{-1}) of free CP had been treated for 24 h (Fig. S2).

The results of Fig. 4 indicated that the TA-MSN-carboxylate-CP complexes showed a highly anti-proliferative effect through the induction of cell apoptosis. The observation of cell morphology showed that the cell membranes were very intact and we did not find the cell necrosis from the cell lysis. We inferred that the treatment of TA-MSN-carboxylate-CP complexes only triggered the apoptosis pathway and that no unexpected necrosis cell death was induced. For an anticancer approach, cellular death can occur by either necrosis or apoptosis while apoptosis is a better approach than the necrosis pathway because necrosis usually caused the cell membrane to break and further released cytokines which trigger the inflammatory response and cause a poor prognosis in chemotherapy. To evaluate the anticancer effect, we used a sulforhodamine B assay to examine the inhibitive effects of cell proliferation after the treatment of free CP and pH sensitive TA-MSN-carboxylate-CP complexes. The results showed that the modification of pH sensitive carboxylate-CP complexes in TA-MSN surfaces can efficiently inhibit the cell growth of HT-29 cells in a concentration dependent manner with the 50% growth inhibition (GI_{50}) of 29.2 μg mL^{-1} of TA-MSN-carboxylate-CP samples (Fig. 5b). The loading percentages of CP molecules in pH-sensitive TA-MSN-carboxylate-CP complexes are 10.25% (wt%) so we can calculate that the GI_{50} of the TA-MSN-carboxylate-CP complexes is 3.0 μg mL^{-1} of the free CP concentration. We also examined the anti-proliferative effect of free CP molecules in the HT-29 cancer cell lines while a higher GI_{50} (61.7 μg mL^{-1}) was observed (Fig. 5a). Our results showed that pH sensitive carboxylate-CP complexes modified in TA-MSN surfaces have higher efficacy against the proliferation of cancer cell lines and displayed twenty times more than free CP molecules. We preferred an enhancement of anti-proliferative effects of the pH-sensitive TA-MSN-carboxylate-CP complexes to the high cellular uptake of the nanoparticles through endocytosis which can deliver large amounts of CP complexes into the cytoplasm. However, the low anti-proliferative activity of free CP molecules may come from the low delivery efficiency of free drug molecules because it only enters the cell through simple diffusion. In addition, an extra enhancement of CP release of the pH-sensitive TA-MSNs-carboxylate-CP complexes into the cytoplasm was contributed from the pH-sensitive hydrazone bond which can hydrolyze CP complexes inside endosomes and the release of CP-complexes can further escape endosome to activate CP complexes and induce cell apoptosis.

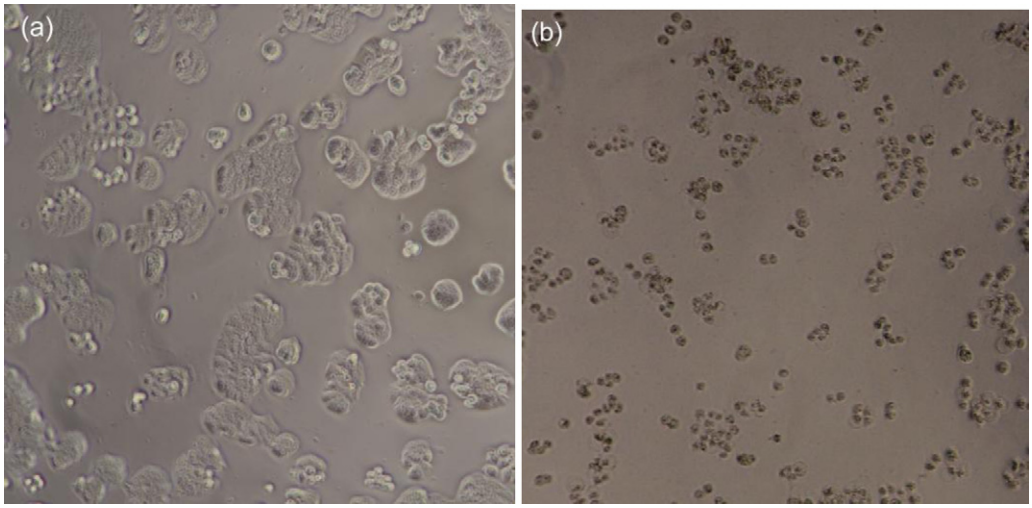

Fig. 4. Cells were incubated in the (a) absence or (b) presence of 50 μg mL^{-1} of TA-MSN-carboxylate-CP complexes for 24 h. Then, the cell cytotoxicity was detected by microscopic morphological examination.

3.4. TA-MSN-carboxylate-CP induced the apoptotic cell death

To determine whether the inhibition of cell proliferation by pH-sensitive TA-MSN-carboxylate-CP complexes came from the induction of apoptosis, we measured the DNA fragmentation with different concentration treatments of free CP and TA-MSN-carboxylate-CP complexes. We treated the cells with different concentrations of drug for 24 h, the total genomic DNA was extracted and analyzed by 2.0% agarose gel electrophoresis, and visualized under ultraviolet transillumination after staining with ethidium bromide. When the cells were treated with free CP and TA-MSN-carboxylate-CP complexes in the CP concentration of 5.1 μg mL^{-1}, DNA ladders were just visible (Fig. 6c and f). A gradually increase of CP concentrations from 10.3 to 20.5 μg mL^{-1} showed an increase of DNA fragmentation in dose dependents. The DNA fragmentation became visible in the treatment of TA-MSN-carboxylate-CP complexes at the CP concentration of 20.5 μg mL^{-1} for 24 h (Fig. 6h), while the treatment of free CP in the same concentration only observed a slight DNA fragmentation (Fig. 6e). The above results showed that TA-MSN-carboxylate-CP complexes with 20.5 μg mL^{-1} of CP loading can efficiently induce the cell death and is mainly caused by apoptosis.

Many studies demonstrated that apoptosis requires the induction of endogenous cellular protease. A family of cysteine proteases, which were named caspases were activated in the apoptotic stimulation. Among these caspases, the activation of caspase 3 is important in many cancer cells to execution of apoptosis. To determine the expression of caspase 3 activity from the treatment of various concentrations of TA-MSN-carboxylate-CP samples, we measured a concentration-dependent elevation of caspase 3 activity using colorimetric assay (Fig. 7). Our results showed that TA-MSN-carboxylate-CP samples induced the apoptotic cell death through the activation of caspases leads to the death and resorption of the cell.

3.5. Hemolysis assay

To further evaluate the in vivo toxicity of the pH-sensitive TA-MSN-carboxylate-CP complexes, we used hemolysis assay to measure the damage of RBCs after the treatment of nanoparticle drugs. Because the damage of RBCs can release red hemoglobin, we can measure the absorbance values of hemoglobin at 570 nm to determine the extent of RBC hemolysis. Previously, Haynes et al. indicated that silica nanoparticles with

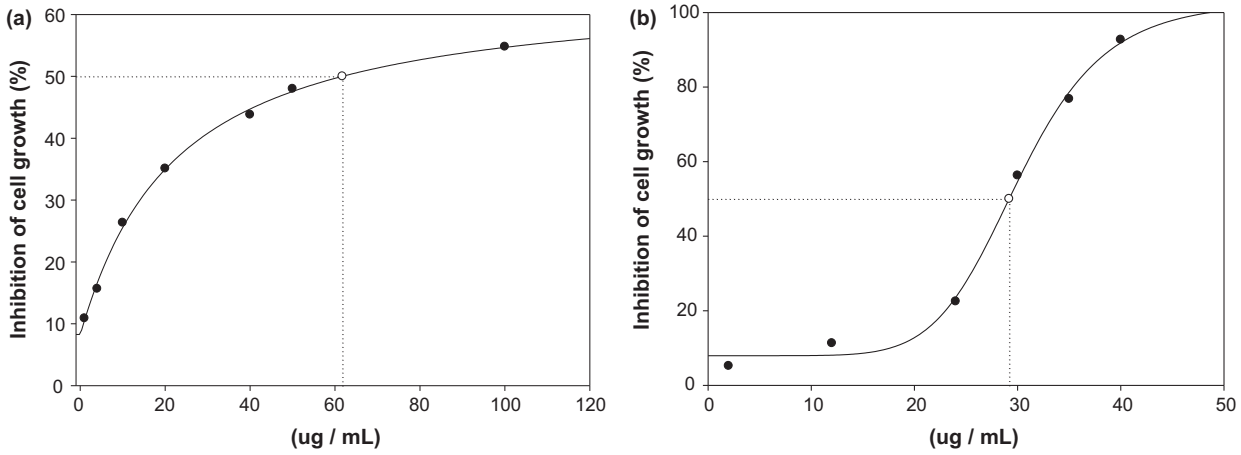

Fig. 5. GI_{50} from the SRB assay of (a) free CP and (b) TA-MSN-carboxylate-CP complexes to HT-29 cells. Various concentrations of TA-MSN-carboxylate-CP complexes were added to cells for 24 h. Then, cells were fixed, stained with SRB, washed with dd-H_2O, subsequently solubilized and finally absorbance was read at a wavelength of 515 nm.

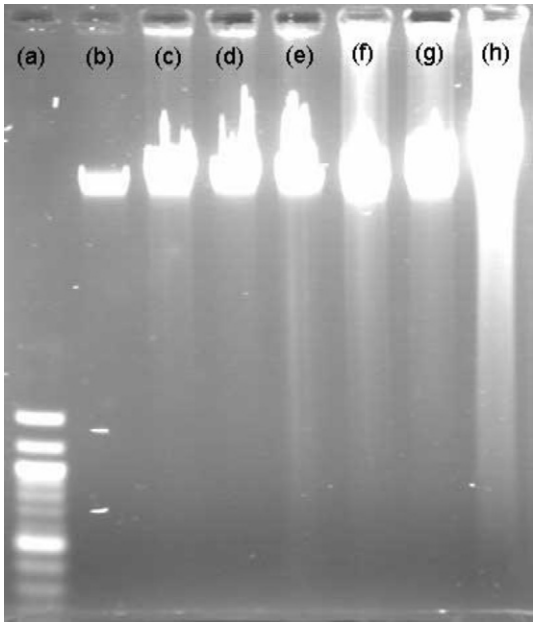

Fig. 6. Induction of DNA fragmentation of free CP molecule and pH-sensitive TA-MSN-carboxylate-CP complexes to colon cancer cells (HT-29) in various concentrations: (a) 100 bp DNA marker and (b) the control experiment without drug treatment; free CP of (c) 5.1 $\mu g\,mL^{-1}$, (d) 10.3 $\mu g\,mL^{-1}$, and (e) 20.5 $\mu g\,mL^{-1}$; TA-MSN-carboxylate-CP complexes with (f) 5.1 $\mu g\,mL^{-1}$, (g) 10.3 $\mu g\,mL^{-1}$, and (h) 20.5 $\mu g\,mL^{-1}$ of corresponding amounts of free CP loading.

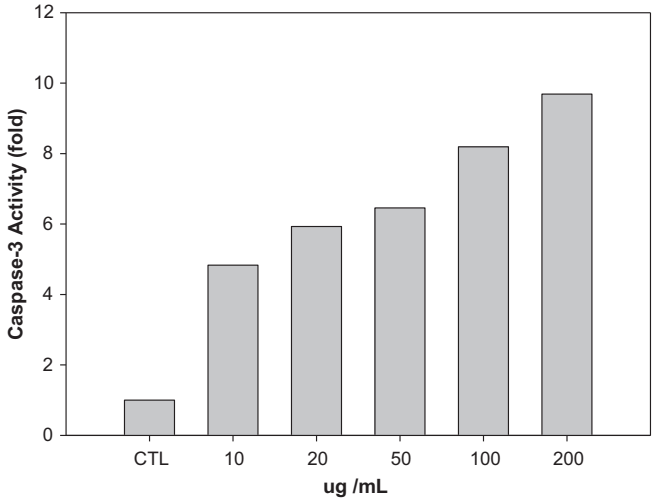

Fig. 7. Involvement of caspases-3 in TA-MSN-carboxylate-CP complexes induced HT-29 apoptosis. Cells were treated without (control) and with various concentrations of TA-MSN-carboxylate-CP complexes for 24 h, and then cells were lysed for the determination of caspase-3 activity.

varied sizes, porous structures and the surface silanol group density effected the nanoparticle–cell interactions and caused red blood cell membrane damage in a concentrated manner (Lin and Haynes, 2010). We treated various concentrations (3.125–1600 $\mu g\,mL^{-1}$) of pH-sensitive TA-MSN-carboxylate samples and TA-MSN-carboxylate-CP complexes to RBCs for 3 h. As shown in Fig. 8, the exposure of pH-sensitive TA-MSN-carboxylate samples in RBCs did not observe the release of hemoglobin from cell lysis (Fig. 8a); therefore, our design of these pH-sensitive nanocarriers is highly biocompatible and has no cytotoxicity in spite of the treatment in a very high nanoparticle concentration. Fig. 8b shows the hemolysis of RBCs after the treatment of TA-MSN-carboxylate-CP complexes for 3 h. We can observe that in the low concentrations of the nano-drug treatment (3.125–100 $\mu g\,mL^{-1}$), there wasn't noticeable hemolysis of RBCs; however, the high concentration treatments (800–1600 $\mu g\,mL^{-1}$) of TA-MSN- carboxylate-CP complexes showed near 60% of the hemoglobin release (Fig. S3).

Although the percentages of the hemolysis increase under a high concentration treatment of pH-sensitive TA-MSN-carboxylate-CP complexes, our pH sensitive CP nano-drugs showed near 100% of growth inhibition at a very low concentration (40 $\mu g\,mL^{-1}$). Our results demonstrated that the pH-sensitive TA-MSN-carboxylate-CP complexes are highly biocompatible, have high drug released efficiency and released specificity which can improve the traditional CP formulation of the chemotherapy. Our previous studies of the in vivo biodistribution also demonstrated that MSN with a highly positive charge can quickly be excreted from the liver into the gastrointestinal tract (Souris et al., 2010). Other researches also indicated the degradation behavior of mesoporous silica in simulated body fluid and urinary excretion of MSNs (He et al., 2011). The use of MSN as a nano-delivery platform in the practical clinical translation showed its feasibility and applicability because many

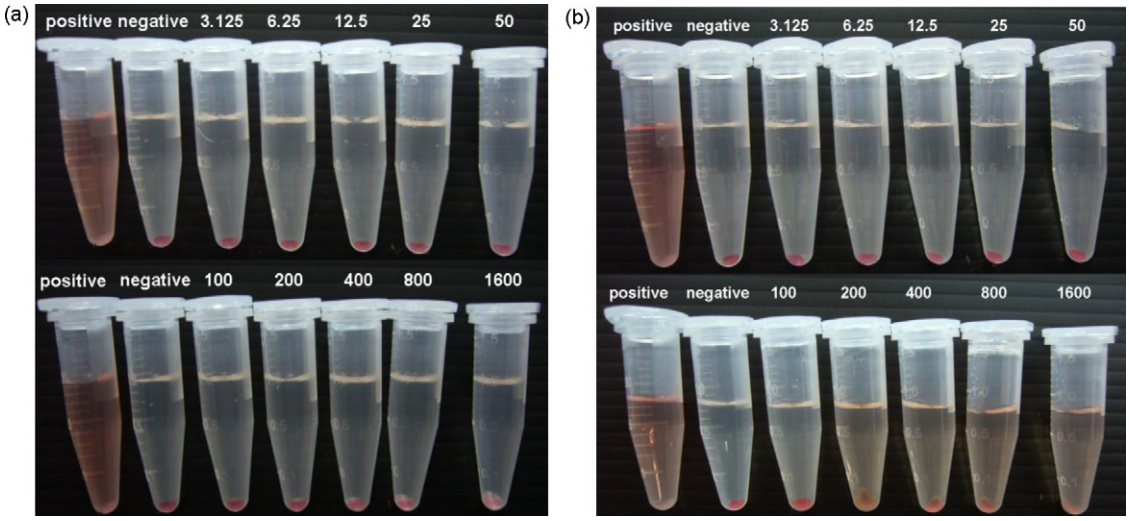

Fig. 8. Photographs of the RBC hemolysis after treatment of various concentrations of (a) TA-MSN-carboxylate and (b) TA-MSN-carboxylate-CP complexes for 3 h. The red hemoglobin in the supernatant indicated the damage of RBCs. dd-H_2O and PBS are used as positive and negative controls, respectively. (For interpretation of the references to color in this figure legend, the reader is referred to the web version of the article.)

studies have determined the biodegradation and excretion of MSN. Thus, the use of pH-sensitive TA-MSN-carboxylate-CP complexes as a highly efficient therapeutic has the potential to be developed for cancer therapy in clinical applications through the increase of therapeutic efficiency while decreasing the side effects.

4. Conclusion

We propose a new pH-sensitive controlled release of CP molecules by coordination of hydroxo-substituted CP with the carboxylate-modified TA-MSN surfaces through a pH-sensitive hydrazone bond. The conjugation of CP-carboxylate complexes through this hydrazone bond can specially release the CP-carboxylate complexes under the endosomal (or lysosomal) environments. Our novel drug delivery platform offers a number of attractive features such as (1) sustained release of potentially toxic CP molecules, (2) decreased non-specific release from enzymatic hydrolysis, (3) increased cellular endocytosis through the incorporation of TA groups in the framework of MSNs, and (4) increased therapeutic effects with decreased side effects. Therefore, the traditional CP formulations for chemotherapy, which usually undergoes dose limiting, low solubility, a lack of in vivo circulation, and nerve toxicity can be efficiently solved through the novel formulation of the pH-sensitive controllable release of CP molecules. The intrinsic accumulation of MSNs in tumor tissues through the EPR effect can especially release highly toxic drugs within tumors, but with nearly none of the side effects that arise from premature drug release. Moreover, the combination of the intrinsically large drug payload and typical endosomal proton densities of MSNs enables the localized, sustained release of CP complexes within diseased tissues.

Acknowledgment

This work was supported by a research grant from the National Science Council of Taiwan (NSC 99-2113-M-259-006-MY2).

Appendix A. Supplementary data

Supplementary data associated with this article can be found, in the online version, at doi:10.1016/j.ijpharm.2012.03.026.

References

Aznar, E., Marcos, M.D., Martinez-Manez, R., Sancenon, F., Soto, J., Amoros, P., Guillem, C., 2009. pH- and photo-switched release of guest molecules from mesoporous silica supports. J. Am. Chem. Soc. 131, 6833–6843.

Bernardos, A., Mondragon, L., Aznar, E., Marcos, M.D., Martinez-Manez, R., Sancenon, F., Soto, J., Barat, J.M., Perez-Paya, E., Guillem, C., Amoros, P., 2010. Enzyme-responsive intracellular controlled release using nanometric silica mesoporous supports capped with saccharides. ACS Nano 4, 6353–6368.

Bhirde, A.A., Patel, V., Gavard, J., Zhang, G.F., Sousa, A.A., Masedunskas, A., Leapman, R.D., Weigert, R., Gutkind, J.S., Rusling, J.F., 2009. Targeted killing of cancer cells in vivo and in vitro with EGF-directed carbon nanotube-based drug delivery. ACS Nano 3, 307–316.

Brigger, I., Dubernet, C., Couvreur, P., 2002. Nanoparticles in cancer therapy and diagnosis. Adv. Drug Deliv. Rev. 54, 631–651.

Cauda, V., Argyo, C., Schlossbauer, A., Bein, T., 2010. Controlling the delivery kinetics from colloidal mesoporous silica nanoparticles with pH-sensitive gates. J. Mater. Chem. 20, 4305–4311.

Chang, B.S., Guo, J., Liu, C.Y., Qian, J., Yang, W.L., 2010. Surface functionalization of magnetic mesoporous silica nanoparticles for controlled drug release. J. Mater. Chem. 20, 9941–9947.

Chen, C.E., Geng, J., Pu, F., Yang, X.J., Ren, J.S., Qu, X.G., 2011a. Polyvalent nucleic acid/mesoporous silica nanoparticle conjugates: dual stimuli-responsive vehicles for intracellular drug delivery. Angew. Chem. Int. Ed. 50, 882–886.

Chen, J., Wang, W., Xu, Y.Q., Zhang, X.H., 2011b. Slow-release formulation of a new biological pesticide, pyoluteorin, with mesoporous silica. J. Agric. Food Chem. 59, 307–311.

Coll, C., Mondragon, L., Martinez-Manez, R., Sancenon, F., Marcos, M.D., Soto, J., Amoros, P., Perez-Paya, E., 2011. Enzyme-mediated controlled release systems by anchoring peptide sequences on mesoporous silica supports. Angew. Chem. Int. Ed. 50, 2138–2140.

Etrych, T., Chytil, P., Jelinkova, M., Rihova, B., Ulbrich, K., 2002. Synthesis of HPMA copolymers containing doxorubicin bound via a hydrazone linkage. Effect of spacer on drug release and in vitro cytotoxicity. Macromol. Biosci. 2, 43–52.

Ferrari, M., 2005. Cancer nanotechnology: opportunities and challenges. Nat. Rev. Cancer 5, 161–171.

Ferris, D.P., Lu, J., Gothard, C., Yanes, R., Thomas, C.R., Olsen, J.C., Stoddart, J.F., Tamanoi, F., Zink, J.I., 2011. Synthesis of biomolecule-modified mesoporous silica nanoparticles for targeted hydrophobic drug delivery to cancer cells. Small 7, 1816–1826.

Gan, Q., Lu, X.Y., Yuan, Y.A., Qian, J.C., Zhou, H.J., Lu, X., Shi, J.L., Liu, C.S., 2011. A magnetic, reversible pH-responsive nanogated ensemble based on Fe_3O_4 nanoparticles-capped mesoporous silica. Biomaterials 32, 1932–1942.

Gao, C.B., Zheng, H.Q., Xing, L., Shu, M.H., Che, S.N., 2010a. Designable coordination bonding in mesopores as a pH-responsive release system. Chem. Mater. 22, 5437–5444.

Gao, Q., Xu, Y., Wu, D., Sun, Y.H., Li, X.A., 2009. pH-responsive drug release from polymer-coated mesoporous silica spheres. J. Phys. Chem. C 113, 12753–12758.

Gao, W.W., Chan, J.M., Farokhzad, O.C., 2010. pH-responsive nanoparticles for drug delivery. Mol. Pharm. 7, 1913–1920.

Giri, S., Trewyn, B.G., Stellmaker, M.P., Lin, V.S.Y., 2005. Stimuli-responsive controlled-release delivery system based on mesoporous silica nanorods capped with magnetic nanoparticles. Angew. Chem. Int. Ed. 44, 5038–5044.

Gu, J.L., Su, S.S., Li, Y.S., He, Q.J., Zhong, F.Y., Shi, J.L., 2010. Surface modification-complexation strategy for cisplatin loading in mesoporous nanoparticles. J. Phys. Chem. Lett. 1, 3446–3450.

Hartono, S.B., Qiao, S.Z., Jack, K., Ladewig, B.P., Hao, Z.P., Lu, G.Q., 2009. Improving adsorbent properties of cage-like ordered amine functionalized mesoporous silica with very large pores for bioadsorption. Langmuir 25, 6413–6424.

He, Q.J., Zhang, Z.W., Gao, F., Li, Y.P., Shi, J.L., 2011. In vivo biodistribution and urinary excretion of mesoporous silica nanoparticles: effects of particle size and PEGylation. Small 7, 271–280.

Heikkila, T., Salonen, J., Tuura, J., Hamdy, M.S., Mul, G., Kumar, N., Salmi, T., Murzin, D.Y., Laitinen, L., Kaukonen, A.M., Hirvonen, J., Lehto, V.P., 2007. Mesoporous silica material TUD-1 as a drug delivery system. Int. J. Pharm. 331, 133–138.

Hsiao, J.K., Tsai, C.P., Chung, T.H., Hung, Y., Yao, M., Liu, H.M., Mou, C.Y., Yang, C.S., Chen, Y.C., Huang, D.M., 2008. Mesoporous silica nanoparticles as a delivery system of gadolinium for effective human stem cell tracking. Small 4, 1445–1452.

Hu, S.H., Liu, T.Y., Huang, H.Y., Liu, D.M., Chen, S.Y., 2008. Magnetic-sensitive silica nanospheres for controlled drug release. Langmuir 24, 239–244.

Kim, J., Kim, H.S., Lee, N., Kim, T., Kim, H., Yu, T., Song, I.C., Moon, W.K., Hyeon, T., 2008. Multifunctional uniform nanoparticles composed of a magnetite nanocrystal core and a mesoporous silica shell for magnetic resonance and fluorescence imaging and for drug delivery. Angew. Chem. Int. Ed. 47, 8438–8441.

Knezevic, N.Z., Trewyn, B.G., Lin, V.S.Y., 2011. Light- and pH-responsive release of doxorubicin from a mesoporous silica-based nanocarrier. Chem. Eur. J. 17, 3338–3342.

Lebret, V., Raehm, L., Durand, J.O., Smaihi, M., Werts, M.H.V., Blanchard-Desce, M., Methy-Gonnod, D., Dubernet, C., 2010. Folic acid-targeted mesoporous silica nanoparticles for two-photon fluorescence. J. Biomed. Nanotechnol. 6, 176–180.

Lee, C.H., Lo, L.W., Mou, C.Y., Yang, C.S., 2008. Synthesis and characterization of positive-charge functionalized mesoporous silica nanoparticles for oral drug delivery of an anti-inflammatory drug. Adv. Funct. Mater. 18, 3283–3292.

Lee, J.E., Lee, N., Kim, H., Kim, J., Choi, S.H., Kim, J.H., Kim, T., Song, I.C., Park, S.P., Moon, W.K., Hyeon, T., 2010. Uniform mesoporous dye-doped silica nanoparticles decorated with multiple magnetite nanocrystals for simultaneous enhanced magnetic resonance imaging, fluorescence imaging, and drug delivery. J. Am. Chem. Soc. 132, 552–557.

Lin, Y.S., Haynes, C.L., 2010. Impacts of mesoporous silica nanoparticle size, pore ordering, and pore integrity on hemolytic activity. J. Am. Chem. Soc. 132, 4834–4842.

Lin, Y.S., Tsai, C.P., Huang, H.Y., Kuo, C.T., Hung, Y., Huang, D.M., Chen, Y.C., Mou, C.Y., 2005. Well-ordered mesoporous silica nanoparticles as cell markers. Chem. Mater. 17, 4570–4573.

Liu, C.Y., Guo, J., Yang, W.L., Hu, J.H., Wang, C.C., Fu, S.K., 2009. Magnetic mesoporous silica microspheres with thermo-sensitive polymer shell for controlled drug release. J. Mater. Chem. 19, 4764–4770.

Lu, F., Wu, S.H., Hung, Y., Mou, C.Y., 2009. Size effect on cell uptake in well-suspended, uniform mesoporous silica nanoparticles. Small 5, 1408–1413.

Malik, N., Evagorou, E.G., Duncan, R., 1999. Dendrimer-platinate: a novel approach to cancer chemotherapy. Anticancer Drugs 10, 767–776.

Mamaeva, V., Rosenholm, J.M., Bate-Eya, L.T., Bergman, L., Peuhu, E., Duchanoy, A., Fortelius, L.E., Landor, S., Toivola, D.M., Linden, M., Sahlgren, C., 2011. Mesoporous silica nanoparticles as drug delivery systems for targeted inhibition of notch signaling in cancer. Mol. Ther. 19, 1538–1546.

Muharnmad, F., Guo, M.Y., Qi, W.X., Sun, F.X., Wang, A.F., Guo, Y.J., Zhu, G.S., 2011. pH-triggered controlled drug release from mesoporous silica nanoparticles via intracelluar dissolution of ZnO nanolids. J. Am. Chem. Soc. 133, 8778–8781.

Prabaharan, M., Grailer, J.J., Pilla, S., Steeber, D.A., Gong, S.Q., 2009. Gold nanoparticles with a monolayer of doxorubicin-conjugated amphiphilic block copolymer for tumor-targeted drug delivery. Biomaterials 30, 6065–6075.

Rieter, W.J., Pott, K.M., Taylor, K.M.L., Lin, W.B., 2008. Nanoscale coordination polymers for platinum-based anticancer drug delivery. J. Am. Chem. Soc. 130, 11584.

Rosenholm, J.M., Peuhu, E., Bate-Eya, L.T., Eriksson, J.E., Sahlgren, C., Linden, M., 2010. Cancer-cell-specific induction of apoptosis using mesoporous silica nanoparticles as drug-delivery vectors. Small 6, 1234–1241.

Sauer, A.M., Schlossbauer, A., Ruthardt, N., Cauda, V., Bein, T., Brauchle, C., 2010. Role of endosomal escape for disulfide-based drug delivery from colloidal mesoporous silica evaluated by live-cell imaging. Nano Lett. 10, 3684–3691.
Schlossbauer, A., Dohmen, C., Schaffert, D., Wagner, E., Bein, T., 2011. pH-responsive release of acetal-linked melittin from SBA-15 mesoporous silica. Angew. Chem. Int. Ed. 50, 6828–6830.
Song, S.W., Hidajat, K., Kawi, S., 2007. pH-controllable drug release using hydrogel encapsulated mesoporous silica. Chem. Commun., 4396–4398.
Souris, J.S., Lee, C.H., Cheng, S.H., Chen, C.T., Yang, C.S., Ho, J.A.A., Mou, C.Y., Lo, L.W., 2010. Surface charge-mediated rapid hepatobiliary excretion of mesoporous silica nanoparticles. Biomaterials 31, 5564–5574.
Sun, G.Y., Chang, Y.P., Li, S.H., Li, Q.Y., Xu, R., Gu, J.M., Wang, E.B., 2009. pH-responsive controlled release of antitumour-active polyoxometalate from mesoporous silica materials. Dalton Trans., 4481–4487.
Sun, J.T., Hong, C.Y., Pan, C.Y., 2010. Fabrication of PDEAEMA-coated mesoporous silica nanoparticles and pH-responsive controlled release. J. Phys. Chem. C 114, 12481–12486.
Suwalski, A., Dabboue, H., Delalande, A., Bensamoun, S.F., Canon, F., Midoux, P., Saillant, G., Klatzmann, D., Salvetat, J.P., Pichon, C., 2010. Accelerated achilles tendon healing by PDGF gene delivery with mesoporous silica nanoparticles. Biomaterials 31, 5237–5245.
Tao, Z.M., Toms, B., Goodisman, J., Asefa, T., 2010. Mesoporous silica microparticles enhance the cytotoxicity of anticancer platinum drugs. ACS Nano 4, 789–794.
Taylor, A., Krupskaya, Y., Kramer, K., Fussel, S., Klingeler, R., Buchner, B., Wirth, M.P., 2010. Cisplatin-loaded carbon-encapsulated iron nanoparticles and their in vitro effects in magnetic fluid hyperthermia. Carbon 48, 2327–2334.
Torney, F., Trewyn, B.G., Lin, V.S.Y., Wang, K., 2007. Mesoporous silica nanoparticles deliver DNA and chemicals into plants. Nat. Nanotechnol. 2, 295–300.
Tourne-Peteilh, C., Lerner, D.A., Charnay, C., Nicole, L., Begu, S., Devoisselle, J.M., 2003. The potential of ordered mesoporous silica for the storage of drugs: the example of a pentapeptide encapsulated in a MSU-Tween 80. ChemPhysChem 4, 281.
Uchino, H., Matsumura, Y., Negishi, T., Koizumi, F., Hayashi, T., Honda, T., Nishiyama, N., Kataoka, K., Naito, S., Kakizoe, T., 2005. Cisplatin-incorporating polymeric micelles (NC-6004) can reduce nephrotoxicity and neurotoxicity of cisplatin in rats. Br. J. Cancer 93, 678–687.
Vallet-Regi, M., Balas, F., Arcos, D., 2007. Mesoporous materials for drug delivery. Angew. Chem. Int. Ed. 46, 7548–7558.
Vallet-Regi, M., Colilla, M., Izquierdo-Barba, I., 2008. Bioactive mesoporous silicas as controlled delivery systems: application in bone tissue regeneration. J. Biomed. Nanotechnol. 4, 1–15.
Vallhov, H., Gabrielsson, S., Stromme, M., Scheynius, A., Garcia-Bennett, A.E., 2007. Mesoporous silica particles induce size dependent effects on human dendritic cells. Nano Lett. 7, 3576–3582.
Van Speybroeck, M., Mellaerts, R., Mols, R., Do Thi, T., Martens, J.A., Van Humbeeck, J., Annaert, P., Van den Mooter, G., Augustijns, P., 2010. Enhanced absorption of the poorly soluble drug fenofibrate by tuning its release rate from ordered mesoporous silica. Eur. J. Pharm. Sci. 41, 623–630.
Wang, L.S., Wu, L.C., Lu, S.Y., Chang, L.L., Teng, I.T., Yang, C.M., Ho, J.A.A., 2010. Biofunctionalized phospholipid-capped mesoporous silica nanoshuttles for targeted drug delivery: improved water suspensibility and decreased nonspecific protein binding. ACS Nano 4, 4371–4379.
Wang, S.B., 2009. Ordered mesoporous materials for drug delivery. Micropor. Mesopor. Mater. 117, 1–9.
Wang, T.T., Chai, F., Fu, Q., Zhang, L.Y., Liu, H.Y., Li, L., Liao, Y., Su, Z.M., Wang, C.A., Duan, B.Y., Ren, D.X., 2011. Uniform hollow mesoporous silica nanocages for drug delivery in vitro and in vivo for liver cancer therapy. J. Mater. Chem. 21, 5299–5306.
Wu, H.X., Liu, G., Zhang, S.J., Shi, J.L., Zhang, L.X., Chen, Y., Chen, F., Chen, H.R., 2011. Biocompatibility, MR imaging and targeted drug delivery of a rattle-type magnetic mesoporous silica nanosphere system conjugated with PEG and cancer-cell-specific ligands. J. Mater. Chem. 21, 3037–3045.
Xie, Y.M., Aillon, K.L., Cai, S.A., Christian, J.M., Davies, N.M., Berkland, C.J., Forrest, M.L., 2010. Pulmonary delivery of cisplatin–hyaluronan conjugates via endotracheal instillation for the treatment of lung cancer. Int. J. Pharm. 392, 156–163.
Xue, J.M., Shi, M., 2004. PLGA/mesoporous silica hybrid structure for controlled drug release. J. Control. Release 98, 209–217.
Yang, Q., Wang, S.H., Fan, P.W., Wang, L.F., Di, Y., Lin, K.F., Xiao, F.S., 2005. pH-responsive carrier system based on carboxylic acid modified mesoporous silica and polyelectrolyte for drug delivery. Chem. Mater. 17, 5999–6003.
Yuan, L., Tang, Q.Q., Yang, D., Zhang, J.Z., Zhang, F.Y., Hu, J.H., 2011. Preparation of pH-responsive mesoporous silica nanoparticles and their application in controlled drug delivery. J. Phys. Chem. C 115, 9926–9932.
Zhang, Y.Z., Zhang, J.H., Jiang, T.Y., Wang, S.L., 2011. Inclusion of the poorly water-soluble drug simvastatin in mesocellular foam nanoparticles: drug loading and release properties. Int. J. Pharm. 410, 118–124.
Zhao, Y.L., Li, Z.X., Kabehie, S., Botros, Y.Y., Stoddart, J.F., Zink, J.I., 2010. pH-operated nanopistons on the surfaces of mesoporous silica nanoparticles. J. Am. Chem. Soc. 132, 13016–13025.
Zheng, H.Q.Z.H.Q., Gao, C.B., Peng, B.W., Shu, M.H., Che, S.N., 2011. pH-responsive drug delivery system based on coordination bonding in a mesostructured surfactant/silica hybrid. J. Phys. Chem. C 115, 7230–7237.